Check for updates

Received: 9 December 2025 | Revised: 5 March 2026 | Accepted: 2 April 2026

DOI: 10.4218/etrij.2025-0509

ETRI Journal WILEY

ORIGINAL ARTICLE

Empirical investigation of directional beamforming for sub-THz propagation loss based on 255 GHz indoor office and industrial environment measurements

Juyul Lee | **Myung-Don Kim** | **Jae-Joon Park** | **Heon Kook Kwon**

Radio Research Division, Electronics and Telecommunications Research Institute (ETRI), Daejeon, Republic of Korea

Correspondence
Juyul Lee, Radio Research Division, Electronics and Telecommunications Research Institute (ETRI), Daejeon, Republic of Korea.
Email: juyul@etri.re.kr

Funding information
This research was supported by the Institute for Information & Communications Technology Planning & Evaluation (IITP) grant funded by the Korean government (MSIT) (2021-0-00103, "Research and development of technologies for utilization of THz frequency band and evaluation of electromagnetic safety").

Abstract

This study presents an empirical investigation of propagation loss characteristics at 255 GHz in indoor office and industrial environments, focusing on the directional beamforming performance under varying beam alignment conditions. Using a wideband channel sounder equipped with 30° Tx and 10° Rx horn antennas, three beamforming schemes are analyzed: (1) the optimal best-beam pair, (2) *n*-th ordered beam pairs, and (3) randomly selected beam pairs. While the best-beam propagation loss is well characterized by conventional distance-dependent models (alpha-beta and close-in propagation loss models), the *n*-th ordered and random beam pairs exhibit converging excess-loss behaviors. Notably, line-of-sight (LoS) links incur substantial penalties under random beam alignments, whereas non-LoS links incur smaller penalties, reflecting the inherent multipath diversity available in indoor channels. These findings provide experimentally grounded insights into the trade-offs between beam management overhead and system performance, establishing a foundation for interference analysis and beam management design of future sub-THz wireless networks.

KEYWORDS
beamforming, propagation loss, propagation measurements, sub-THz propagation

1 | INTRODUCTION

Beamforming is a key enabling technology for the utilization of millimeter-wave (mmWave) and sub-THz frequency bands[1]; however, it typically requires elaborate alignment protocols and introduces substantial complexity [1–3]. While its benefits for link performance have been well established, the extent of performance degradation without precise beam alignment remains unclear. This study empirically investigates not only the achievable propagation loss[2] under optimal beam steering but also the excess loss associated with non-ideal beamforming, with a particular focus on indoor environments where relatively rich multipath propagation may provide

[1]The mmWave band spans frequencies from 30 to 300 GHz. The sub-THz band is generally used to denote the higher portion of this range, specifically 100 to 300 GHz [1].

[2]Throughout the paper, the term *propagation loss* is used in the context of directional beamforming, rather than *path loss*, as the latter may imply the exclusion of antenna beamforming effects.

This is an Open Access article distributed under the term of Korea Open Government License (KOGL) Type 4: Source Indication + Commercial Use Prohibition + Change Prohibition (http://www.kogl.or.kr/info/licenseTypeEn.do).
1225-6463/$ © 2026 ETRI

inherent directional diversity [4]. Specifically, 255 GHz is considered because it falls within the candidate sub-THz International Mobile Telecommunications (IMT) bands identified by ITU-R for WRC-31 (102–109.5, 151.5–164, 167–174.8, 209–226, and 252–275 GHz) [5], where beamforming is indispensable.

Recently, numerous indoor and outdoor propagation measurement studies in the sub-THz band have been reported, providing a growing experimental foundation for sub-THz wireless systems [6–8] (and references therein). Representative studies include factory and urban measurement campaigns conducted at 142 GHz [9, 10], which demonstrate diverse propagation characteristics in various sub-THz scenarios. Furthermore, several indoor campaigns have targeted frequencies above 200 GHz by employing directional horn antennas with systematic angular measurements [11–15]. Despite these advances, most existing studies have primarily focused on optimal beam alignment or omnidirectional synthesis. In practical systems, however, beam directions are not always perfectly aligned due to training overhead, mobility, blockage dynamics, and hierarchical beam search procedures [16]. As such, propagation behavior associated with non-optimal beam directions and unintended spatial coupling remains insufficiently quantified from a measurement-based perspective, particularly at frequencies near 255 GHz.

Motivated by these practical beam management challenges, we extend the analysis to non-optimal beam pairs[3]: the *n*-th ordered and randomly selected beam pairs. The *n*-th ordered beams are analyzed by quantifying the excess loss relative to the optimal direction, revealing the performance degradation that may arise during practical beam training, beam tracking, and beam recovery procedures [16, 17]. Randomly oriented beamforming is also analyzed to provide insight into the performance cost of avoiding beam alignment overhead and to offer a statistical means for interference assessment in spectrum sharing studies [18].

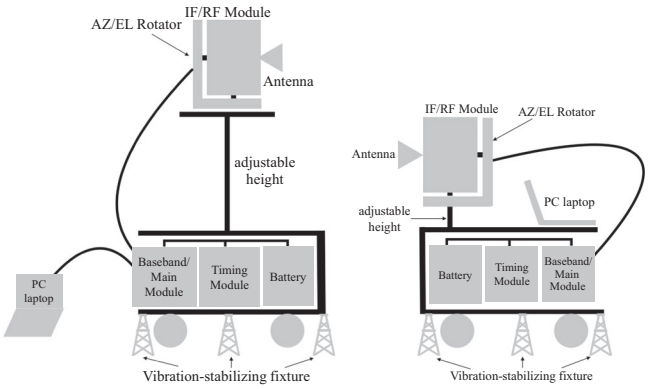
In the literature, several studies have explored the impact of beam patterns and random beamforming, from different perspectives. For instance, Zhang and others [19] investigated the effect of directional beam patterns on sub-THz channels, focusing on the number of useful beams and beamformed channel similarity to develop design guidelines. Lee and others [20] and Heath and others [21] introduced the notion of random directional beamforming for mmWave communications; however, these prior studies were primarily theoretical or simulation-based, focusing on multiuser diversity. Although recent measurement campaigns have shown that indoor environments may exhibit richer multipath structures than commonly assumed [4], the performance robustness of directional beamforming under imperfect alignment remains insufficiently explored using empirical data. To investigate this, our study adopts a measurement-based approach, with measurements conducted in two representative indoor environments—office and industrial scenarios—featuring diverse scatterers and reflective surfaces, which have been recognized as standard indoor scenarios by 3GPP and ITU-R [22, 23]. Although the analysis is based on horn-antenna configurations, the methodology can be extended to array-based implementations [24]. To the best of our knowledge, this study is the first to analyze *n*-th ordered and random directional beamforming using real-world sub-THz measurements, providing a new empirical perspective.

[3]The analysis does not assume intentional operation using non-optimal beams; instead, it models realistic beam misalignment conditions encountered during practical beam management procedures.

2 | MEASUREMENT CAMPAIGN

The measurements were conducted using a correlation-based 255 GHz channel sounder with a 5 GHz bandwidth. Building upon the time-domain correlation framework of our 159 GHz sounder [25, 26], we employed a PN sequence length of 8191 chips, with a delay resolution of 0.2 ns and a CIR sampling interval of 0.05 ns. The maximum RF transmit power was 0 dBm, with the transmitter (Tx) and receiver (Rx) synchronized via rubidium clocks. As shown in Figure 1, each Tx and Rx unit comprises an IF/RF module mounted on a dual-axis azimuth/elevation (AZ/EL) rotator, as well as a baseband/main module, a timing module, a battery unit, a PC laptop controller, and an antenna.

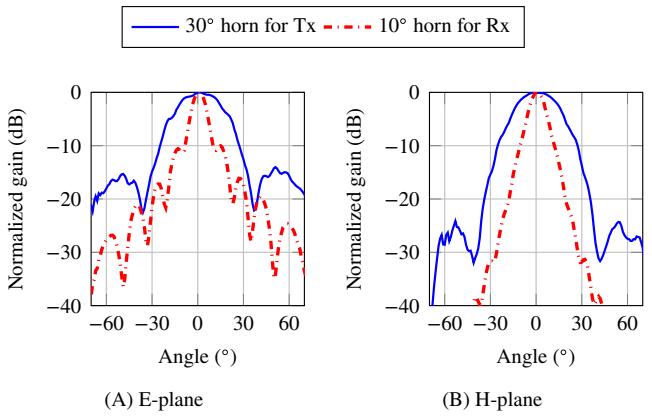
Rotationally scanning horn antennas were employed: a 30° half-power beamwidth (HPBW) horn at the Tx



(A) Tx unit (B) Rx unit

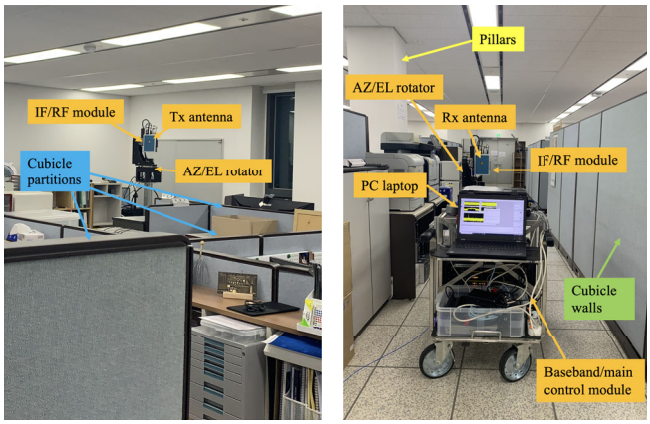
FIGURE 1 255 GHz channel sounder configuration.

22337326, 0, Downloaded from https://onlinelibrary.wiley.com/doi/10.4218/etrij.2025-0509 by Electronics and Telecommunications, Wiley Online Library on [29/10/2026]. See the Terms and Conditions (https://onlinelibrary.wiley.com/terms-and-conditions) on Wiley Online Library for rules of use; OA articles are governed by the applicable Creative Commons License



(A) E-plane (B) H-plane

FIGURE 2 Measured antenna radiation patterns.



(A) Tx installation (B) Rx installation

FIGURE 3 Office environment measurement setup.

(15.0 dBi gain) and a 10° HPBW horn at the Rx (24.7 dBi gain). The measured radiation patterns are shown in Figure 2. The antennas were rotated in non-overlapping steps corresponding to their respective beamwidths. In the azimuth plane, the Rx and Tx scanned 360° in 36 and 12 steps, respectively. To reduce measurement time, the elevation scan was restricted to $-10°, 0°$, and $+10°$. In total, 1296 directional combinations (12 Tx AZ × 36 Rx AZ × 3 Rx EL) were measured for each Tx–Rx link. Over-the-air calibration was performed multiple times on each measurement day to ensure stable system performance, given the sensitivity of high-frequency components to environmental factors (for example, temperature, humidity, pressure, etc.) [26–28].

Measurements were performed in two representative indoor environments—office and industrial—commonly used as reference deployment scenarios in channel modeling studies [22]. The office setting represents a structured indoor workspace dominated by partitions and furniture, while the industrial setting includes dense metallic structures relevant to emerging industrial IoT deployments [29].

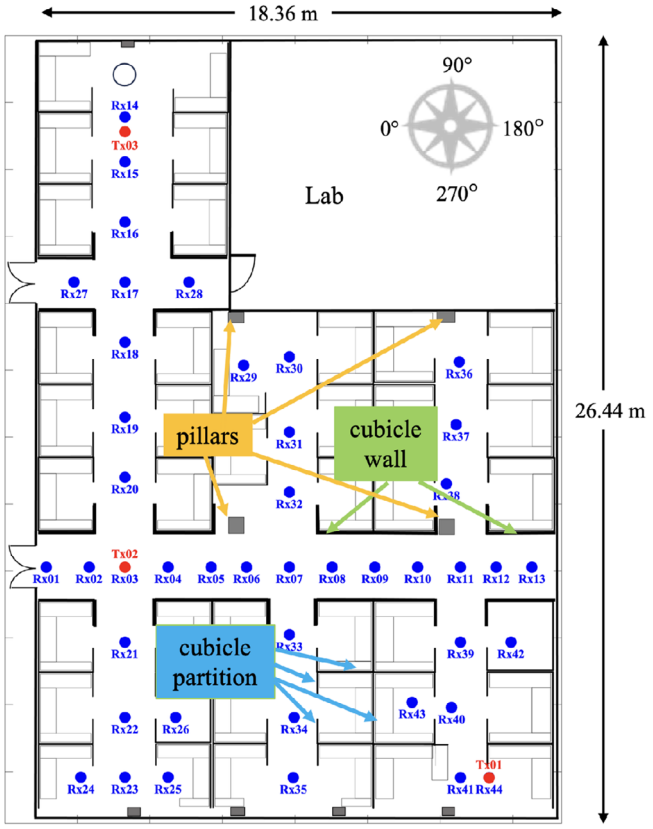


FIGURE 4 Office measurement layout with Tx and Rx positions.

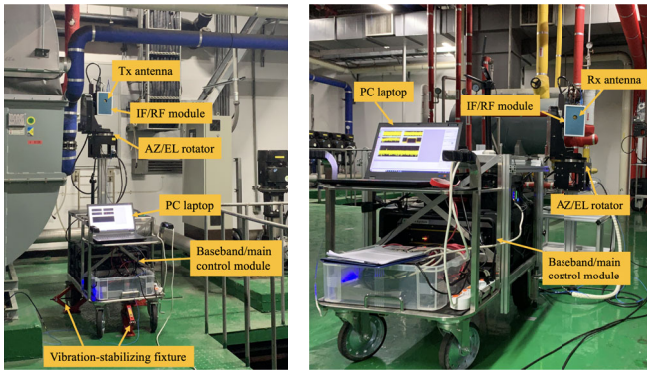
The Tx and Rx antenna heights were fixed at 1.96 m and 1.20 m, respectively. Measurements were conducted during off-hours to ensure static conditions, and the LoS/NLoS status was identified by visual inspection.

The office measurement campaign was conducted in an 18.36 m × 26.44 m cubicle area with a ceiling height of 2.70 m inside an ETRI office building [4, 14] (Figures 3 and 4), containing pillars, cubicle walls/partitions, and various office furniture. As illustrated in the figure, the Tx antenna assembly was positioned above the cubicle partitions, while the Rx antenna assembly was placed below them. Data were collected from 3 Tx and 44 Rx positions, yielding 41 LoS and 50 NLoS links after excluding short-range links that fell outside the Tx antenna's elevation beam coverage (Figure 4).

The industrial measurement campaign was conducted in a 22.5 m × 12.0 m machine room with a significantly higher ceiling of 5.20 m at an ETRI facility (Figures 5 and 6). This environment was filled with extensive metallic equipment, pipes, and railings that could create strong reflection and shadowing effects. Measurements from 3 Tx and 40 Rx positions yielded 27 LoS and 31 NLoS links for analysis.

Notably, the measurement results were subject to spatial sampling limitations inherent to the measurement

22337326, 0, Downloaded from https://onlinelibrary.wiley.com/doi/10.4218/etrij.2025-0509 by Electronics and Telecommunications, Wiley Online Library on [29/10/2026]. See the Terms and Conditions (https://onlinelibrary.wiley.com/terms-and-conditions) on Wiley Online Library for rules of use; OA articles are governed by the applicable Creative Commons License



(A) Tx installation (B) Rx installation

FIGURE 5 Industrial environment measurement setup.

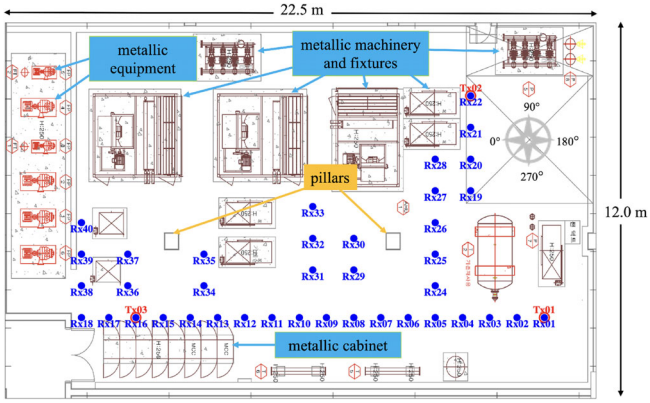


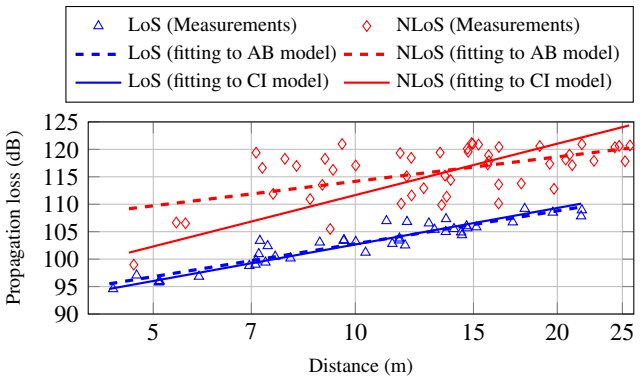
FIGURE 6 Industrial measurement layout with Tx/Rx positions.

setup. While discrete angular scanning and Tx–Rx locations may not capture all possible propagation realizations, the collected data provide statistically meaningful characterization of the directional propagation behavior. Future work with denser sampling may further refine the statistical characterization.

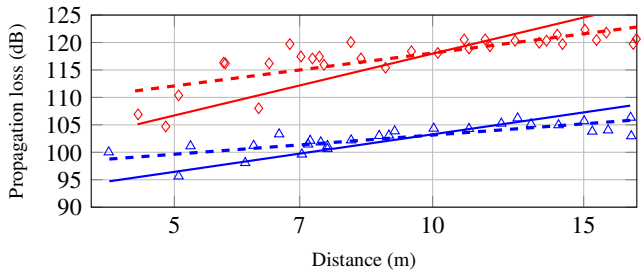
3 | DIRECTIONAL PROPAGATION LOSS MEASUREMENTS

3.1 | Optimal (best-beam) pair

The rotational scanning procedure yielded 1296 directional beam pairs per Tx–Rx link, obtained by steering the Tx antenna over 12 azimuth angles and the Rx antenna over 108 directions (36 azimuth × 3 elevation angles). First, we consider the *best-beam* scheme, defined as the directional combination that maximizes received power. Figure 7 shows the directional propagation loss as a function of the Tx–Rx separation distance d (m), and its



(A) Office environment measurements



(B) Industrial environment measurements

FIGURE 7 Directional propagation loss measurements.

least-squares fits to the alpha-beta (AB) and close-in free space (CI) models [30],

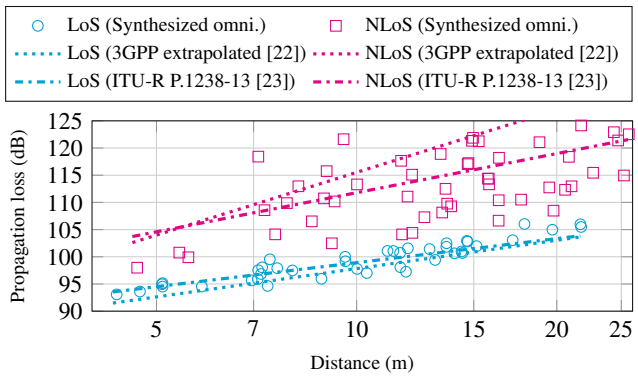
$$\mathrm{PL}^{\mathrm{AB}}(d) = 10\alpha \log_{10} d + \beta, \ \ (\mathrm{dB}), \tag{1}$$

$$\mathrm{PL}^{\mathrm{CI}}(d) = 10n \log_{10} d + \mathrm{FSPL}_{1\mathrm{m}}, \ \ (\mathrm{dB}), \tag{2}$$

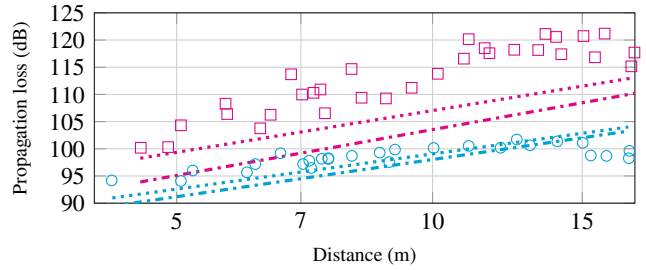
where α and β are the AB model parameters, n is the CI model propagation-loss exponent, $\mathrm{FSPL}_{1\mathrm{m}} = 20\log_{10}(4\pi \times 255 \times 10^9/c)$ is the free space loss at 1 m, and c denotes the speed of light [30]. The estimated parameters are $\alpha = 1.99, \beta = 82.90, n = 2.21$ (office LoS); $\alpha = 1.48, \beta = 99.37, n = 3.11$ (office NLoS); $\alpha = 1.16, \beta = 91.54, n = 2.27$ (industrial LoS); and $\alpha = 1.99, \beta = 98.18, n = 3.74$ (industrial NLoS). As shown in Figure 7, the fitted curves clearly distinguish the LoS and NLoS conditions in both environments and capture the distance-dependent behavior of the directional propagation loss.

Numerous measurement campaigns have been conducted above 100 GHz (see [6–8] and references therein). However, a direct comparison between the directional measurements of this study and existing results is nontrivial because prior studies employed different beamwidths and operated at frequencies other than 255 GHz. To enable a more consistent comparison, synthesized omnidirectional propagation losses were generated using the

22337326, 0, Downloaded from https://onlinelibrary.wiley.com/doi/10.4218/etrij.2025-0509 by Electronics and Telecommunications, Wiley Online Library on [29/10/2026]. See the Terms and Conditions (https://onlinelibrary.wiley.com/terms-and-conditions) on Wiley Online Library for rules of use; OA articles are governed by the applicable Creative Commons License



(A) Office environment measurements



(B) Industrial environment measurements

FIGURE 8 Synthesized omnidirectional propagation loss, with 3GPP/ITU-R models for comparison.

technique[4] described in [33, §4 in Annex 1], as shown in Figure 8. These synthesized omnidirectional losses are generally lower than the directional losses since more multipath components can be captured with omnidirectional transmission/reception [34]. Compared with the other cases, the office NLoS scenario exhibits smaller differences between directional and omnidirectional losses, which can be attributed to fewer multipaths arriving from non-dominant directions. The figure also compares the synthesized omnidirectional loss with standardized models: 3GPP TR 38.901[5] [22] and Recommendation ITU-R P.1238 [23]. The industrial NLoS curves of both 3GPP and ITU-R P.1238[6] models exhibit relatively low propagation loss levels, suggesting that further discussion in the standardization bodies may be required, supported

[4]We note that various other synthesizing methods have been proposed in the literature, but they generally yield similar loss characteristics [27, 31, 32].

[5]The applicable frequency range of the 3GPP model is up to 100 GHz. The curves here were obtained by extrapolating the model to 255 GHz.

[6]The measurement data used in this study were submitted to the ITU-R Study Group 3 Data Bank to contribute to the revision of Recommendation ITU-R P.1238-13. However, for industrial NLoS environments, substantially more measurement datasets below 100 GHz than above 100 GHz were used to derive the model parameters, leading to a bias toward lower frequency conditions.

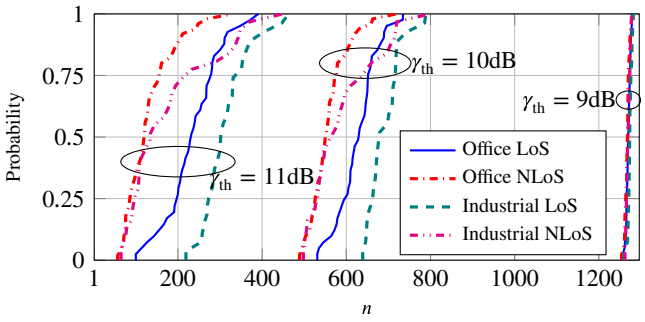


FIGURE 9 Cumulative distribution function (CDF) of outage probability in terms of n, where n denotes the n-th best directional combination at which outage begins.

by more extensive measurement data at these frequencies. Propagation modeling for emerging frequency bands is typically refined through iterative comparison between measurements and analytical models within standardization activities. Recent efforts in model validation and multi-frequency channel characterization, including those supporting simulator evolution and consistency verification [35–37], follow this measurement-driven refinement approach. Therefore, this measurement-based study provides experimentally derived propagation characteristics at 255 GHz that may support future model validation and channel simulator development, such as NYUSIM [38].

3.2 | *n*-th ordered directional beam pair

When beamforming is employed, beam management typically considers not only the strongest beam direction but also several candidate beams to enhance robustness against sudden link blockages or misalignment [16, 17]. In this subsection, we investigate the n-th directional propagation loss behavior extracted from 1296 measured beam-pair combinations per link. These combinations are sorted in ascending order of loss, where $n = 1$ represents the optimal direction.

Before analyzing the n-th ordered behavior, we examine outage probabilities derived from the data. By defining outage as the received signal-to-noise (SNR) falling below a given threshold γ_{th}, Figure 9 shows the cumulative distribution function (CDF) of the outage probability versus n for $\gamma_{th} = 9$, 10, and 11 dB. It is seen that even small changes in γ_{th} cause noticeable differences in the outage performance. For instance, at $\gamma_{th} = 10$ dB, LoS links in both environments outperform NLoS links, with median outage starting points of approximately $n = 630 - 750$ for LoS and $n = 550$ for NLoS. The industrial environment consistently outperforms the office, as its more reflective machinery creates a richer multipath environment. At

22337326, 0, Downloaded from https://onlinelibrary.wiley.com/doi/10.4218/etrij.2025-0509 by Electronics and Telecommunications, Wiley Online Library on [29/10/2026]. See the Terms and Conditions (https://onlinelibrary.wiley.com/terms-and-conditions) on Wiley Online Library for rules of use; OA articles are governed by the applicable Creative Commons License

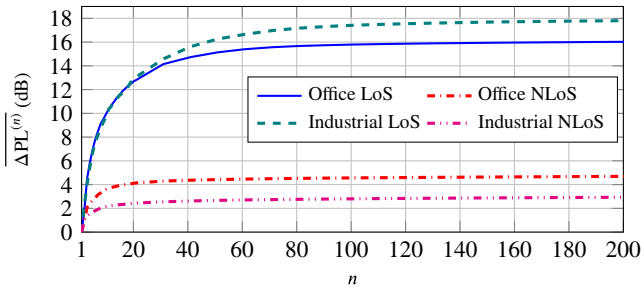


FIGURE 10 Average differential propagation loss relative to that in the optimal direction.

$\gamma_{th} = 9$ dB, outage occurs at relatively large n and shows negligible variation across all scenarios. No outage was observed for $\gamma_{th} \leq 8$ in our measurements. It should be noted, however, that outage performance would vary under different antenna beamwidth configurations. In our setup with 30° Tx and 10° Rx beamwidths in indoor office and industrial environments, outages were rarely observed under non-optimal beam combinations, which supports the suitability for investigating n-th ordered and even random directional beamforming.

We now analyze the n-th ordered behavior by quantifying the performance degradation as the beam direction deviates from the optimal direction. To characterize this degradation, we define the excess loss incurred under n-th ordered directional beamforming, relative to that obtained under the optimal beam direction as the *differential propagation loss*:

$$\Delta PL^{(n)} = PL^{(n)} - PL^{(1)} \ \text{(dB)}, \tag{3}$$

where $PL^{(n)}$ denotes the n-th smallest directional propagation loss, and $PL^{(1)}$ corresponds to the optimal (minimum loss) direction. This relative metric isolates the beamforming effect by removing variations caused by distance and environmental geometry, thereby allowing a fairer comparison across different links. Figure 10 shows the average differential propagation loss, $\overline{\Delta PL^{(n)}}$, across all measured links in the office and industrial environments.[7] As shown in Figure 10, $\overline{\Delta PL^{(n)}}$ increases with n and eventually saturates at a saturation level that depends on the environment and LoS/NLoS condition. LoS links exhibit consistently higher differential losses than that of NLoS links, implying that power is more concentrated in the optimal direction; by contrast, power is more dispersed under NLoS conditions. The LoS links in both environments show similar values up to $n \approx 20$; however, beyond this, the industrial environment exhibits higher values. This can be attributed to the increased dominance of specular reflections from large metallic machinery, which concentrates power into fewer dominant beams. In contrast, for NLoS links, the office environment yields higher differential losses across all n. This is likely due to fewer strong reflections compared to the richer scattering found in the industrial environment, which distributes power more evenly across multiple paths. It should be noted, however, that these observations are empirical; different antenna configurations and environments may yield different absolute values.

[7]The overbar, $\overline{(\cdot)}$, denotes the averaging operation.

3.3 | Randomly selected directional beam pair

This subsection analyzes randomly selected directional beam pairs as a theoretical reference to provide insight into spatial performance statistics and interference behavior under imperfect or exploratory beam alignment. Interference analysis is vital for frequency allocation, spectrum planning [18], and the design of interference-limited communication systems [39, 40]. However, the impact of sub-THz directional beamforming on unintended users remains insufficiently quantified through real-world measurements. In practical systems, interference often arises from unintended signal power delivery to non-target receivers via side lobes, reflections, or beam misalignment.

To investigate this behavior from a propagation perspective, we examine random directional beamforming, where the Tx and Rx antennas are steered toward randomly selected directions without intentional beam alignment. The resulting performance is then compared with that of the optimal beamforming. Although practical interference beams could be constrained to specific angular regions depending on deployment scenarios and beam-management procedures, the random beam selection considered in this study provides a measurement-based statistical reference for characterizing unintended signal coupling. Consequently, this analysis could serve as a baseline for evaluating interference statistics and spatial coexistence in sub-THz systems [18].

3.3.1 | Random directional beamforming to a single direction

Previously, the index (n) was used to denote the sorted directional propagation loss, with $n = 1$ corresponding to the optimal beam direction. To analyze random beamforming, we introduce an unsorted index m that represents a directional combination among the 1296 measured beam pairs. In this context, single-direction

22337326, 0, Downloaded from https://onlinelibrary.wiley.com/doi/10.4218/etrij.2025-0509 by Electronics and Telecommunications, Wiley Online Library on [29/10/2026]. See the Terms and Conditions (https://onlinelibrary.wiley.com/terms-and-conditions) on Wiley Online Library for rules of use; OA articles are governed by the applicable Creative Commons License

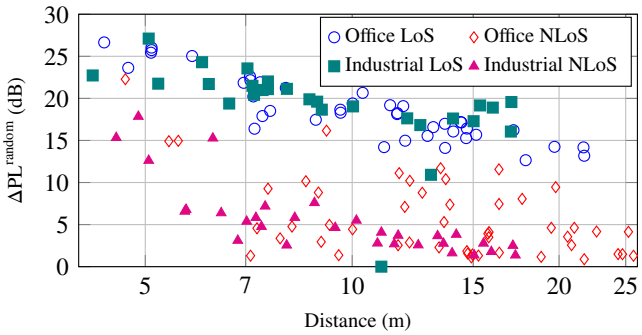


FIGURE 11 Differential propagation loss for a single random directional beamforming realization.

random beamforming refers to selecting a beam index uniformly at random:

$$m \sim \mathcal{U}(\{1,2,...,1296\}), \tag{4}$$

where $\mathcal{U}(X)$ denotes a discrete uniform distribution over the elements of set X.

The resulting performance degradation is quantified by the differential propagation loss:

$$\Delta\mathrm{PL}^{\mathrm{random}} = \mathrm{PL}^{m} - \mathrm{PL}^{(1)}, \tag{5}$$

where PL^{m} is the loss of the randomly selected beam and $\mathrm{PL}^{(1)}$ is the optimal loss. Figure 11 illustrates a realization of the measured differential propagation loss, $\Delta\mathrm{PL}^{\mathrm{random}}$. For short distances (<8 m), $\Delta\mathrm{PL}^{\mathrm{random}}$ tends to decrease with distance, suggesting that the relative importance of beam alignment decreases with distance. Beyond this range, the effect of distance on random beamforming becomes less pronounced. LoS links exhibit higher differential losses than NLoS links, implying a greater potential for performance improvement through beam alignment. The consistently lower differential losses in NLoS links suggest that random beamforming can achieve "reasonable" performance in multipath-rich environments, especially where dominant paths are not relatively stronger than non-dominant paths. Unlike the differential losses for ordered directional beamforming shown in Figure 10, the lack of significant differences between office and industrial environments suggests that random beamforming performance is robust across diverse indoor conditions.

3.3.2 | Random directional beamforming to multiple directions

We extend the random beamforming concept to multiple directions. Let M denote the number of randomly

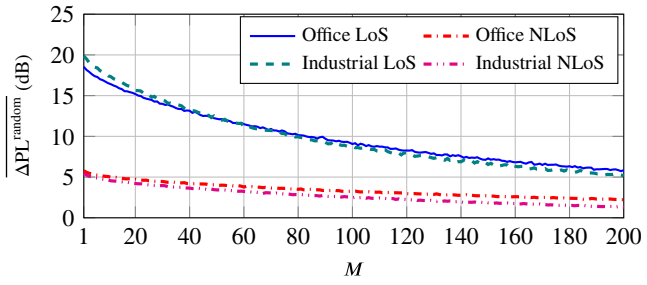


FIGURE 12 Average differential propagation loss of M randomly-oriented directional beamforming.

selected directional combinations drawn from the complete set of 1,296 beam pairs. The selection process can be expressed as:

$$(m_1, m_2, ..., m_M) \sim \mathcal{U}^{M}_{\mathrm{w/o\ repl}}(\{1,2,...,1296\}), \tag{6}$$

where $\mathcal{U}^{M}_{\mathrm{w/o\ repl}}(X)$ represents an M-sized discrete uniform distribution over X, drawn without replacement.[8] Alternative sampling strategies produce similar trends and are therefore omitted for brevity.

Figure 12 shows the average differential propagation loss, $\overline{\Delta\mathrm{PL}^{\mathrm{random}}}$, as a function of M, averaged over all measurement samples and 100 Monte Carlo runs. For LoS links, the differential loss is approximately 18 to 20 dB at $M = 1$ and decreases with M, suggesting an increased likelihood of capturing stronger multipath components as more random beam directions are combined. In contrast, NLoS links exhibit differential losses of approximately 5 to 6 dB at $M = 1$ with a slower decay. Furthermore, the similar trends observed for the office and industrial environments suggest that the effect of M dominates over the effect of environmental differences, while the differences observed between LoS and NLoS cases suggest a stronger directional concentration in LoS cases.

3.3.3 | Beamwidth-dependent random directional beamforming

Thus far, the analysis has considered only the measured antenna beamwidth, $\theta_T = 30^\circ$ and $\theta_R = 10^\circ$, where θ_T and θ_R denote the beamwidths of the Tx and Rx antennas, respectively. Using the beamwidth synthesis techniques described in [33, 34], integer multiples of these beamwidths can be synthesized. It is worthwhile to

[8]Depending on how repeated directions are allowed, several selection strategies can be considered. In this study, we consider allowing all Tx–Rx directional combinations except those in which both antennas employ identical directions.

22337326, 0, Downloaded from https://onlinelibrary.wiley.com/doi/10.4218/etrij.2025-0509 by Electronics and Telecommunications, Wiley Online Library on [29/10/2026]. See the Terms and Conditions (https://onlinelibrary.wiley.com/terms-and-conditions) on Wiley Online Library for rules of use; OA articles are governed by the applicable Creative Commons License

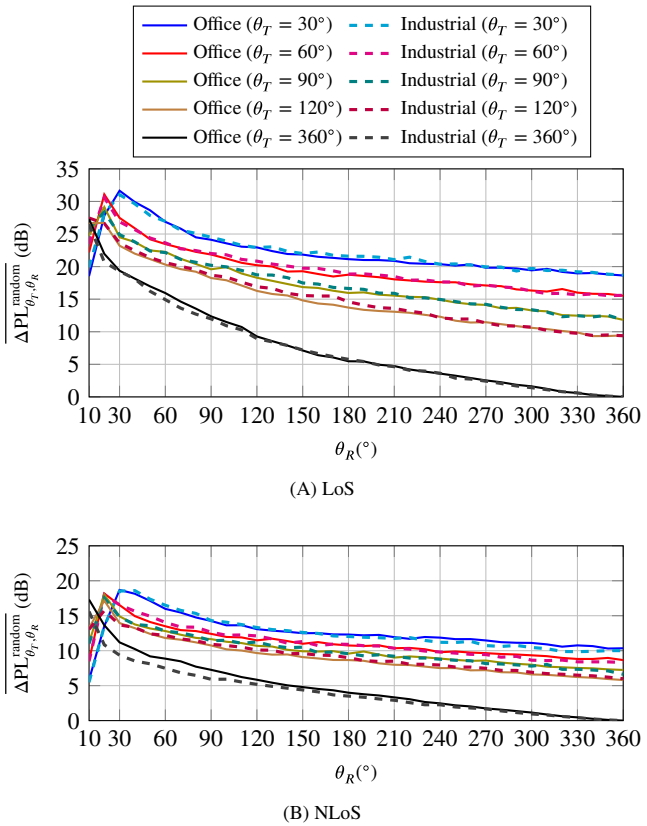
mention that synthesizing beamwidths in the elevation plane is constrained by our measurement rotation scheme. For the Tx, θ_T can be expanded into integer multiples of 30° in the azimuth plane, while the elevation beamwidth remains fixed at 30°. For the Rx, when θ_R is between 10° and 30°, the same beamwidth is applied in both azimuth and elevation. For $\theta_R > 30°$, the elevation beamwidth is fixed at 30° because the antenna was rotated in only three elevation steps, limiting the maximum synthesizable elevation beamwidth to 30°.

When calculating the differential propagation loss in (5), the reference loss $\mathrm{PL}^{(1)}$ must correspond to the specific beamwidths under consideration. This ensures that the metric captures only the loss attributed to random beamforming for the given configuration, that is,

$$\Delta\mathrm{PL}^{\mathrm{random}}_{\theta_T,\theta_R} = \mathrm{PL}^{m}_{\theta_T,\theta_R} - \mathrm{PL}^{(1)}_{\theta_T,\theta_R}. \tag{7}$$

Figure 13 shows the average differential propagation loss, $\overline{\Delta\mathrm{PL}^{\mathrm{random}}_{\theta_T,\theta_R}}$, as a function of the Rx beamwidth (θ_R) for various Tx beamwidths (θ_T), averaged over all measurement samples and 100 Monte Carlo runs. Across both environments for LoS/NLoS links, $\overline{\Delta\mathrm{PL}^{\mathrm{random}}_{\theta_T,\theta_R}}$ generally decreases as θ_R or θ_T increases, since wider beams are more likely to capture stronger multipath components. For small θ_R, an initial increase in differential loss can be observed because the propagation loss for the optimal beam, $\mathrm{PL}^{(1)}_{\theta_T,\theta_R}$, improves rapidly with slight Rx beamwidth widening, while random beamforming improves more gradually. This temporarily increases the differential loss before it decreases with further widening. Differences between the office and industrial environments remain minor, whereas differences between LoS and NLoS are considerable.

From these beamwidth-dependent results for $\Delta\mathrm{PL}^{\mathrm{random}}_{\theta_T,\theta_R}$, it is also interesting to examine the case where an omnidirectional antenna is employed on either the Tx or Rx side, as shown in Figure 14. When the Tx is omnidirectional, as shown in Figure 14a, the average differential loss decreases monotonically with Rx beamwidth. LoS links exhibit higher losses than NLoS links, consistent with the stronger concentration of directional energy along dominant paths. Notably, the reduction from $\theta_R = 10°$ to $\theta_R = 30°$ is steeper than the changes beyond $\theta_R = 30°$. A similar monotonic trend is observed when the Rx is omnidirectional, as shown in Figure 14b.



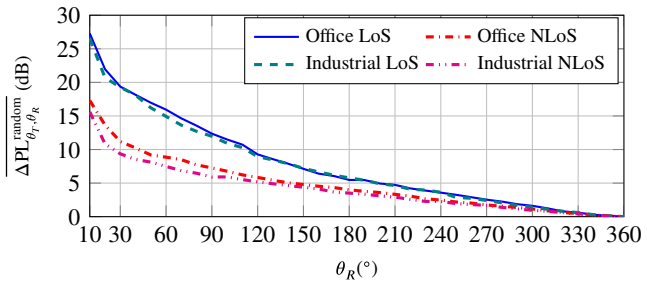
(A) LoS

(B) NLoS

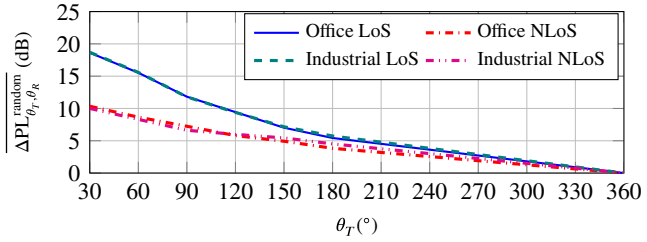
FIGURE 13 Average differential propagation loss versus beamwidths for random directional beamforming.

4 | THEORETICAL INTERPRETATION AND SYSTEM-LEVEL IMPLICATIONS

The observed performance improvement/degradation obtained through directional beamforming can be



(A) When $\theta_T = 360°$ (Tx omnidirectional)



(B) When $\theta_R = 360°$ (Rx omnidirectional)

FIGURE 14 Average differential propagation loss under random directional beamforming when either the Tx or Rx employs an omnidirectional antenna.

22337326, 0, Downloaded from https://onlinelibrary.wiley.com/doi/10.4218/etrij.2025-0509 by Electronics and Telecommunications, Wiley Online Library on [29/10/2026]. See the Terms and Conditions (https://onlinelibrary.wiley.com/terms-and-conditions) on Wiley Online Library for rules of use; OA articles are governed by the applicable Creative Commons License

interpreted as a spatial filtering effect [34]. By steering narrow beams toward dominant propagation paths, the Tx and Rx suppress diffuse scattering components and reduce the multipath energy arriving from non-dominant directions. Consequently, the measured beamforming gain reflects not only antenna directivity but also the angular sparsity characteristics of sub-THz propagation channels.

The differences between the indoor office and industrial environments can be attributed to their distinct electromagnetic properties and physical layouts. Office environments typically feature structured geometries that support relatively stable dominant paths. By contrast, industrial environments are characterized by irregularly distributed metallic machinery, which introduces more intense specular reflections and scattering. These environmental characteristics result in larger variations in propagation loss, as observed in our industrial measurements.

From a modeling perspective, the results are well described by the log-distance propagation formulations given in (1) and (2). The extracted parameters indicate that directional beamforming effectively reduces the apparent propagation loss compared with omnidirectional propagation assumptions when directivity gain is properly accounted for. This observation highlights the necessity of incorporating antenna directivity when developing sub-THz channel models.

Beyond link-level performance, the measurement results provide important implications for interference behavior and spectrum sharing in sub-THz deployments. Directional beamforming limits spatial interference leakage by concentrating the radiated energy within narrow angular regions. As a result, interference between independent links becomes highly dependent on the beam alignment probability rather than solely on the transmission distance. The large differential propagation losses observed for randomly selected beam pairs suggest that unintended beam misalignment naturally reduces the interference coupling among neighboring users. These characteristics indicate that sub-THz systems employing narrow beams can support aggressive spatial reuse and coexistence scenarios, which are essential for future interference- and spectrum-sharing frameworks. Furthermore, the measured propagation trends facilitate predictive evaluation of the interference-limited performance. The experimentally observed beam-dependent loss statistics can be utilized in system-level simulations to estimate interference distributions, evaluate multi-user coexistence strategies, and design beam coordination or beam-selection protocols.

Although this study is measurement-based, the results allow practical performance predictions for indoor deployments near 255 GHz, including link budget estimation, beam alignment requirements, and spatial reuse capability. It should be noted that the objective of this work is not to introduce a new analytical propagation model, but rather to provide experimentally grounded characterization. These measurement results complement existing theoretical studies by supplying realistic parameters and empirical insights necessary for future model development and system-level simulations.

5 | CONCLUSION

This paper presented an empirical study of directional beamforming propagation loss at 255 GHz in indoor office and industrial environments. Using rotationally scanned beam measurements with 30° Tx and 10° Rx beams, the best-beam pair, the n-th ordered pair, and randomly selected pairs were analyzed.

For the best-beam pair, the directional propagation loss in both environments was well characterized by the AB and CI models, while outage was rarely observed under the considered setup, indicating substantial directional diversity in the indoor environments. For the n-th ordered beams, the average differential loss increased with n before reaching a saturation point, with larger asymptotic penalties observed for LoS than for NLoS links. Random beam selection exhibited large differential losses for LoS links (approximately 18–20 dB), but smaller penalties for NLoS links (approximately 5–6 dB), highlighting the role of multipath richness in sustaining link performance. Furthermore, the analysis demonstrated how performance scales with the number of randomly combined directions, beamwidth dependency, and omnidirectional assumptions.

The similarity in differential loss trends for random beamforming across office and industrial environments suggests that the results could be generalized across diverse indoor settings. Although the results are inherently constrained by the empirical nature of the study and specific measurement setup, they provide practical predictive insights for future sub-THz system design. Overall, the findings demonstrate the potential of directional beamforming to exploit multipath diversity, while quantifying the performance cost associated with imperfect beam alignment. Future work will investigate the frequency dependency and broader system-level extensions.

CONFLICT OF INTEREST STATEMENT

The authors declare that there is no conflict of interest.

ORCID

Juyul Lee https://orcid.org/0000-0002-5851-0615
Jae-Joon Park https://orcid.org/0000-0002-8695-8185

22337326, 0, Downloaded from https://onlinelibrary.wiley.com/doi/10.4218/etrij.2025-0509 by Electronics and Telecommunications, Wiley Online Library on [29/10/2026]. See the Terms and Conditions (https://onlinelibrary.wiley.com/terms-and-conditions) on Wiley Online Library for rules of use; OA articles are governed by the applicable Creative Commons License

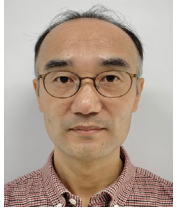
REFERENCES

1. T. S. Rappaport, Y. Xing, O. Kanhere, S. Ju, A. Madanayake, S. Mandal, A. Alkhateeb, and G. C. Trichopoulos, *Wireless communications and applications above 100 GHz: opportunities and challenges for 6G and beyond*, IEEE Access **7** (2019), 78729–78757.
2. S. Kutty and D. Sen, *Beamforming for millimeter wave communications: an inclusive survey*, IEEE Commun. Surv. Tutor. **18** (2016), no. 2, 949–973.
3. Y.-N. R. Li, B. Gao, X. Zhang, and K. Huang, *Beam management in millimeter-wave communications for 5G and beyond*, IEEE Access **8** (2020), 13282–13293.
4. J. Lee, J.-J. Park, K.-W. Kim, H. K. Kwon, and M.-D. Kim, *Measurement-based omnidirectional millimetre-wave and sub-THz, propagation analysis in a large cubicle office environment*, IET Microw. Antennas Propag. **17** (2023), no. 6, 443–453.
5. ITU, Resolution 814, Preliminary agenda for the 2031 World Radiocommunication Conference, 2023. https://www.itu.int/en/ITU-R/study-groups/rcpm/Pages/wrc-31-preliminary-studies.aspx
6. A. Ghosh and M. Kim, *THz channel sounding and modeling techniques: an overview*, IEEE Access **11** (2023), 17823–17856.
7. C. Han, Y. Wang, Y. Li, Y. Chen, N. A. Abbasi, T. Kurner, and A. F. Molisch, *Terahertz wireless channels: a holistic survey on measurement, modeling, and analysis*, IEEE Commun. Surv. Tutor. **24** (2022), no. 3, 1670–1707.
8. D. Serghiou, M. Khalily, T. W. C. Brown, and R. Tafazolli, *Terahertz channel propagation phenomena, measurement techniques and modeling for 6G wireless communication applications: a survey, open challenges and future research directions*, IEEE Commun. Surv. Tutor. **24** (2022), no. 4, 1957–1996.
9. S. Ju, D. Shakya, H. Poddar, Y. Xing, O. Kanhere, and T. S. Rappaport, *142 GHz sub-terahertz radio propagation measurements and channel characterization in factory buildings*, IEEE Trans. Wireless Commun. **23** (2024), no. 7, 7127–7143.
10. D. Shakya, S. Ju, O. Kanhere, H. Poddar, Y. Xing, and T. S. Rappaport, *Radio propagation measurements and statistical channel models for outdoor urban microcells in open squares and streets at 142, 73, and 28 GHz*, IEEE Trans. Antennas Propag. **72** (2024), no. 4, 3580–3595.
11. Y. Chen, C. Han, Z. Yu, and G. Wang, *Channel measurement, characterization, and modeling for terahertz indoor communications above 200 GHz*, IEEE Trans. Wireless Commun. **23** (2024), no. 6, 6518–6532.
12. Y. Wang, X. Zhou, X. Liao, J. Zhang, and J. Zhang, *Channel measurements and multipath characterization for indoor sub-terahertz communication*, IEEE Trans. Wireless Commun. **74** (2025), no. 3, 4393–4407.
13. A. Al-jzari, Y. He, J. Hu, and S. Salous, *Sub-THz and THz channel measurements and characteristic analysis in indoor and outdoor environments for 6G wireless systems*, IEEE Trans. THz Sci. Technol. **15** (2025), no. 6, 976–984.
14. J. Lee, M. D. Kim, J. J. Park, B. S. Kang, and H. K. Kwon, *255 GHz indoor office propagation measurements for path loss and delay spread analysis*, (2025 International Symposium on Antennas and Propagation (ISAP), Fukuoka, Japan), 2025, pp. 1–2.
15. T. Zhang, Y. He, C. Pan, H. Ren, H. Chang, C.-X. Wang, and J. Wang, *Indoor channel measurements and characterization for virtual multiantenna at 260 GHz to 400 GHz*, IEEE Antennas Wireless Propag. Lett. **24** (2025), no. 11, 3841–3845.
16. M. Giordani, M. Polese, A. Roy, D. Castor, and M. Zorzi, *A tutorial on beam management for 3GPP NR at mmWave frequencies*, IEEE Commun. Surv. Tutor. **21** (2019), no. 1, 173–196.
17. M. Li, C. Liu, S. V. Hanly, I. B. Collings, and P. Whiting, *Explore and eliminate: optimized two-stage search for millimeter-wave beam alignment*, IEEE Trans. Wireless Commun. **18** (2019), no. 9, 4379–4393.
18. ITU-R Handbook, *ITU-R propagation prediction methods for interference and sharing studies ITU*, 2012.
19. P. Zhang, M. F. D. Guzman, X. Li, X. Cai, K. Haneda, N. Tervo, et al., *Understanding subterahertz radio channels: the impact of beamforming on wireless system design*, IEEE Veh. Technol. Mag. **20** (2025), no. 3, 49–57.
20. G. Lee, Y. Sung, and J. Seo, *Randomly-directional beamforming in millimeter-wave multiuser MISO downlink*, IEEE Trans. Wireless Commun. **15** (2016), no. 2, 1086–1100.
21. R. W. Heath, N. Gonzalez-Prelcic, S. Rangan, W. Roh, and A. M. Sayeed, *An overview of signal processing techniques for millimeter wave MIMO systems*, IEEE J. Sel. Topics Signal Process. **10** (2016), no. 3, 436–453.
22. 3GPP, *Study on channel model for frequencies from 0.5 to 100 GHz*, V17.1.0, 3GPP TR 38.901, 2023.
23. Rec. ITU-R P.1238-13, *Propagation data and prediction methods for the planning of indoor radiocommunication systems and radio local area networks in the frequency range 300 MHz to 450 GHz ITU*, 2025.
24. J. Lee, M.-D. Kim, and J.-J. Park, *Empirical investigation of array beamforming effects on received power and delay spread characteristics based on 159-GHz measurements*, IEEE Wireless Commun. Lett. **14** (2025), no. 2, 430–434.
25. M. D. Kim, H. K. Kwon, K. W. Kim, J. Lee, and J. J. Park, *Implementation and performance evaluation of wideband channel sounder at 159 GHz*, (International Conference on Information and Communication Technology Convergence (ICTC), Jeju Island, Republic of Korea), 2022, pp. 2322–2325. DOI 10.1109/ICTC55196.2022.9952403
26. J. Lee, J.-J. Park, K.-W. Kim, M.-D. Kim, and H. K. Kwon, *159-GHz propagation measurement and analysis in urban microcellular environment for 6G*, IEEE Wireless Commun. Lett. **12** (2023), no. 2, 277–281.
27. N. A. Abbasi, J. Gomez-Ponce, R. Kondaveti, A. Kumar, E. Bhagat, R. N. S. Rao, et al., *THz band channel measurements and statistical modeling for urban microcellular environments*, IEEE Trans. Wireless Commun. **23** (2024), no. 7, 6719–6734.
28. M. D. Al-Dabbagh, D. Ulm, T. Doeker, D. Dupleich, A. Ebert, R. S. Thomä, et al., *Characterization of sub-THz channel sounding systems in OTA measurement scenarios using a vector network analyzer*, IEEE Trans. Antennas Propag. **73** (2025), no. 6, 3943–3958.
29. D. C. Nguyen, M. Ding, P. N. Pathirana, A. Seneviratne, J. Li, D. Niyato, O. Dobre, and H. V. Poor, *6G Internet of things: a comprehensive survey*, IEEE Internet Things J. **9** (2022), no. 1, 359–383.
30. S. Sun, T. S. Rappaport, T. A. Thomas, A. Ghosh, H. C. Nguyen, I. Z. Kovacs, I. Rodriguez, O. Koymen, and A. Partyka, *Investigation of prediction accuracy, sensitivity, and parameter stability of large-scale propagation path loss models*

22337326, 0, Downloaded from https://onlinelibrary.wiley.com/doi/10.4218/etrij.2025-0509 by Electronics and Telecommunications, Wiley Online Library on [29/10/2026]. See the Terms and Conditions (https://onlinelibrary.wiley.com/terms-and-conditions) on Wiley Online Library for rules of use; OA articles are governed by the applicable Creative Commons License

for 5G wireless communications, IEEE Trans. Veh. Technol. **65** (2016), no. 5, 2843–2860.
31. S. Sun, G. R. MacCartney, M. K. Samimi, and T. S. Rappaport, *Synthesizing omnidirectional antenna patterns, received power and path loss from directional antennas for 5G millimeter-wave communications*, (2015 IEEE Global Communications Conference (GLOBECOM), San Diego, CA, USA), 2015, pp. 1–7.
32. K. Haneda, S. L. H. Nguyen, J. Jarvelainen, and J. Putkonen, *Estimating the omni-directional pathloss from directional channel sounding*, (2016 10th European Conference on Antennas and Propagation (EuCAP), Davos, Switzerland), 2016, pp. 1–5.
33. Recommendation ITU-R P.1407-8, *Multipath propagation and parameterization of its characteristics*, 2021.
34. J. Lee, M.-D. Kim, J.-J. Park, and Y. J. Chong, *Field-measurement-based received power analysis for directional beamforming millimeter-wave systems: effects of beamwidth and beam misalignment*, ETRI J. **40** (2018), no. 1, 26–38.
35. H. Poddar, D. Gold, D. Lee, N. Zhang, G. Sridharan, H. Asplund, and M. Shafi, Overview of 3GPP Release 19 study on channel modeling enhancements to TR 38.901 for 6G, arXiv preprint (2025). DOI 10.48550/arXiv.2507.19266
36. H. Poddar, T. Yoshimura, and A. Ishii, *Validation of 3GPP TR 38.901 indoor hotspot path loss model based on measurements conducted 6.75, 16.95, 28, and 73 GHz for 6G and beyond*, (IEEE 101st Vehicular Technology Conference (VTC2025-Spring), Oslo, Norway), 2025, pp. 1–6.
37. H. Poddar and A. Chowdary, *Single and multi-frequency path loss models for indoor hotspot scenario based on measurements conducted at 6.75, 16.95, 28, 73 and 142 GHz*, arXiv preprint (2025). DOI 10.48550/arXiv.2509.07331
38. H. Poddar, S. Ju, D. Shakya, and T. S. Rappaport, *A tutorial on NYUSIM: sub-terahertz and millimeter-wave channel simulator for 5G, 6G and beyond*, IEEE Commun. Surv. Tutor. **26** (2024), no. 2, 824–857.
39. H. Dai, A. Molisch, and H. Poor, *Downlink capacity of interference-limited MIMO systems with joint detection*, IEEE Trans. Wireless Commun. **3** (2004), no. 2, 442–453.
40. A. Tusha and H. Arslan, *Interference burden in wireless communications: a comprehensive survey from PHY layer perspective*, IEEE Commun. Surv. Tutor. **27** (2025), no. 4, 2204–2246.

AUTHOR BIOGRAPHIES



Juyul Lee received his PhD degree in electrical engineering from the University of Minnesota, Twin Cities, USA, in 2010. He was with the Agency for Defense Development, Republic of Korea, from 1998 to 2000. Since 2000, he has been with the Electronics and Telecommunications Research Institute, Republic of Korea, where he is currently a principal researcher in the Radio Research Division. His research interests include wireless channel modeling, millimeter-wave and sub-THz propagation, machine learning, and information theory. He has contributed extensively to ITU-R recommendations and reports, focusing on the development and extension of short-range indoor and outdoor propagation models. He is currently the chairperson of the ITU-R Correspondence Group 3K-6, which is responsible for studying the impact of higher frequencies (up to 450 GHz) on propagation models and related characteristics. He is a senior member of the IEEE.



Myung-Don Kim received his BS and MS degrees in electronic engineering from Dong-A University, Busan, Republic of Korea, in 1993 and 1995, respectively. Since 1995, he has been with the Electronics and Telecommunications Research Institute, Republic of Korea, where he is currently a principal researcher. Throughout his career, he participated in numerous projects, including the commercialization of CDMA systems and the development of video telephony services for WCDMA terminals. Since 2006, he has served as a project leader for the development of wireless channel models for 4G, 5G, and 6G systems. Since 2009, he has been actively involved in standardization activities within 3GPP and ITU-R Study Group 3 (Radiowave Propagation). He currently serves as a rapporteur and chair of the Draft Group in ITU-R Working Party 3K, where he leads the development of Recommendation ITU-R P.1411, which addresses propagation prediction models for short-range outdoor environments. His research interests include the development of wideband channel sounders and channel models for next-generation wireless communications, spanning from microwave to sub-THz bands.



Jae-Joon Park received the BS and MS degrees in control and instrumentation from Chung-Ang University, Seoul, Republic of Korea in 1997 and 1999, respectively. Since 1999, he has been with Electronics and Telecommunications Research Institute, Daejeon, Republic of Korea, where he is currently a principal researcher. His professional career focused on the development of smart antennas for FDD/TDD WCDMA system, the WiBro system for broadband wireless internet services, and wideband wireless channel model for 4G, 5G and 6G. His current research interests include channel measurements and modeling of surface wave communications in metallic environments.

22337326, 0, Downloaded from https://onlinelibrary.wiley.com/doi/10.4218/etrij.2025-0509 by Electronics and Telecommunications, Wiley Online Library on [29/10/2026]. See the Terms and Conditions (https://onlinelibrary.wiley.com/terms-and-conditions) on Wiley Online Library for rules of use; OA articles are governed by the applicable Creative Commons License



Heon Kook Kwon received his BS and MS degrees in electronics engineering from the School of Engineering, Chungnam National University, Daejeon, Republic of Korea, in 1997 and 1999, respectively. Since 2004, he has been with the Electronics and Telecommunications Research Institute, Daejeon, Republic of Korea, where he is currently a principal researcher. His professional career was focused on the development of RF systems for wireless communication. His current research interests include RF system design and technologies for the next-generation wireless communications.

How to cite this article: J. Lee, M.-D. Kim, J.-J. Park, and H. K. Kwon, *Empirical investigation of directional beamforming for sub-THz propagation loss based on 255 GHz indoor office and industrial environment measurements*, ETRI Journal (2026), 1–12, DOI 10.4218/etrij.2025-0509

22337326, 0, Downloaded from https://onlinelibrary.wiley.com/doi/10.4218/etrij.2025-0509 by Electronics and Telecommunications, Wiley Online Library on [29/10/2026]. See the Terms and Conditions (https://onlinelibrary.wiley.com/terms-and-conditions) on Wiley Online Library for rules of use; OA articles are governed by the applicable Creative Commons License